RECONSTRUCTING LAGRANGIAN VELOCITY GRADIENTS IN INHOMOGENEOUS TURBULENT FLOWS FROM COARSE-GRAINED SIMULATIONS

Perry L. Johnson & Charles Meneveau
Department of Mechanical Engineering
Johns Hopkins University
Baltimore MD 21218 USA
pjohns86@jhu.edu

ABSTRACT

The detailed dynamics of small particles and droplets in turbulent flows are not directly accessible in standard large-eddy simulations because the relevant small-scale physics is unresolved. This paper aims to demonstrate a technique for recovering unresolved velocity gradients along Lagrangian paths, which are important for a number of micro-physical applications. Stochastic models previously used for Lagrangian velocity gradients in isotropic turbulence are adapted to work alongside large-eddy simulations under the assumption that the unresolved turbulence is approximately locally isotropic. The technique is demonstrated for a turbulent channel flow by explicitly filtering a DNS simulation at $Re_\tau = 1000$ from the Johns Hopkins Turbulence Databases for use as a 'perfect LES' solution. The results of the stochastic model are then compared to particle tracking results from the full DNS solution. This demonstrates that the stochastic models developed for Lagrangian velocity gradients in isotropic turbulence can be implemented as a practical tool for large-eddy simulations in a wide range of engineering and geophysical flows.

INTRODUCTION

Standard large-eddy simulation (LES) techniques aim to accurately simulate a coarse-grained representation of a given high-Reynolds-number turbulent flow (Sagaut, 2006). Knowledge of the fine-scale structure of turbulence is required by many scientific and engineering problems, such as particle dispersion (Sawford, 2001), preferential concentration (Maxey, 1987), polymer stretching (White & Mungal, 2008), droplet and bubble deformation (Maffettone & Minale, 1998), rigid particle rotation (Voth & Soldati, 2017), aggregate break-up (Marchioli & Soldati, 2015), microorganism nutrient uptake (Karp-Boss *et al.*, 1996), and hemolysis (De Tullio *et al.*, 2012).

Some modeling work has been done for simulating particle dispersion in the context of LES by using stochastic models (Mazzitelli *et al.*, 2014) or differential filter deconvolution methods (Park *et al.*, 2015) for mimicking the subgrid scale velocity fluctuations. Little previous work has focused on recovering unresolved velocity gradients, a notable exception being the recent work of Chen *et al.* (2016), who used an Ornstein-Uhlenbeck model for velocity gradient statistics (Pumir & Wilkinson, 2011), which assumes Gaussian statistics for the gradients. At high Reynolds numbers, unresolved velocity gradients are highly non-Gaussian and of much larger in magnitude compared to resolved velocity gradients, which makes it imperative for additional modeling even for qualitative order-of-magnitude success.

Under the long-standing hypothesis of approximate universality and local isotropy of small-scale turbulence at high Reynolds numbers and far from boundaries (Kolmogorov, 1941; Sreenivasan & Antonia, 1997; Pope, 2000), it is expected that accurate modeling of Lagrangian velocity gradients in isotropic turbulence can serve as a basis for a wide range of inhomogeneous flows. Early investigations of the restricted Euler model for Lagrangian velocity gradient dynamics (Vieillefosse, 1982, 1984; Cantwell, 1992) showed that the non-linear self-amplification term with a local, isotropic pressure Hessian accounted for many of the important qualitative features of turbulent velocity gradients, such as the enhanced probability of extreme excursions down the Vieillefosse tail in the Q-R plane and the preferential alignment of the vorticity with the strain-rate eigenvector associated with its intermediate eigenvalue, although it diverges at later time due to a finite-time singularity . While the linear damping closure of Martin *et al.* (1998) failed to prevent this singularity for some initial conditions, further modeling work (Jeong & Girimaji, 2003; Chevillard & Meneveau, 2006) leveraged techniques developed for tetrad dispersion models (Chertkov *et al.*, 1999) to demonstrate the capability of stochastic models with recent-deformation closures to provide realistic stationary statistics. For a review, see Meneveau (2011). Further improvements were made recently by the introduction of a Gaussian fields closure (Wilczek & Meneveau, 2014) and by a framework for closure based on deformation of Gaussian fields from (Johnson & Meneveau, 2016).

In this paper, we construct a Lagrangian stochastic model for the sub-grid velocity gradients from the filtered Navier-Stokes equations. Unclosed terms, such as the pressure Hessian and viscous Laplacian, are treated with models that have been developed for accuracy in isotropic turbulence (Johnson & Meneveau, 2016), under the hypothesis of approximate universality and local isotropy for small-scale turbulence at high Reynolds numbers. The method is demonstrated by considering the velocity gradients along Lagrangian trajectories in a turbulent channel flow using a DNS database solution.

MODEL DEVELOPMENT

Governing Equations

We consider the low-pass filtering operation with filter width Δ,

$$\widetilde{u}_i(\mathbf{x}) = \iiint G(\mathbf{r};\Delta) u_i(\mathbf{x}+\mathbf{r}) d^3 r, \tag{1}$$

decomposing the velocity field into large-scale and small-scale contributions: $u_i = \widetilde{u}_i + u_i'$. Applying the filter operator on the incompressible Navier-Stokes equations leads to the large-eddy simulation equations,

$$\partial_t \widetilde{u}_i + \widetilde{u}_j \partial_j \widetilde{u}_i = -\partial_i \widetilde{p} + \nu \nabla^2 \widetilde{u}_i - \partial_j \sigma_{ij}, \tag{2}$$

together with the incompressibility condition, $\partial_i \widetilde{u}_i = 0$, where $\sigma_{ij} = \widetilde{u_i u_j} - \widetilde{u}_i \widetilde{u}_j$ and spatial variation of the filter width is ignored.

We consider the Lagrangian evolution of velocity gradients given by the gradient of the incompressible Navier-Stokes equations,

$$\tfrac{d}{dt} A_{ij} = -A_{ik} A_{kj} - \partial_i \partial_j p + \nu \nabla^2 A_{ij}, \tag{3}$$

where $\frac{d}{dt} = \partial_t + u_j \partial_j$ is the material derivative. The gradient of the filtered incompressible Navier-Stokes equations gives,

$$\tfrac{d}{dt} \widetilde{A}_{ij} = -\widetilde{A}_{ik} \widetilde{A}_{kj} - \partial_i \partial_j \widetilde{p} + \nu \nabla^2 \widetilde{A}_{ij} - \partial_j \partial_k \sigma_{ik} + u_k' \partial_k \widetilde{A}_{ij}, \tag{4}$$

and the remaining unresolved velocity gradient has the evolution equation,

$$\begin{aligned} \tfrac{d}{dt} A_{ij}' = &-A_{ik}' A_{kj}' - \partial_i \partial_j p' + \nu \nabla^2 A_{ij}' \\ &- A_{ik}' \widetilde{A}_{kj} + \widetilde{A}_{ik} A_{kj}' + \partial_j \partial_k \sigma_{ik} - u_k' \partial_k \widetilde{A}_{ij}. \end{aligned} \tag{5}$$

In the limit of high sub-grid Reynolds number, $Re_{SGS} = \sqrt{15}\sigma_{ii}/\sqrt{\nu\epsilon} \sim \tau_\Delta/\tau_\eta' \gg 1$, where $\tau_\eta' = 1/\sqrt{2\langle S_{ij}' S_{ij}' \rangle}$ and $\tau_\Delta = 1/\sqrt{2\langle \widetilde{S}_{ij} \widetilde{S}_{ij} \rangle}$, the Kolmogorov timescale, $\tau_\eta = 1/\sqrt{2\langle S_{ij} S_{ij} \rangle} \approx \tau_\eta'$, roughly describes the (inverse) magnitude of the unresolved velocity gradients, and the equation for the unresolved velocity gradients can be approximated by the dominant contributions from (5),

$$\tfrac{d}{dt} A_{ij}' = -A_{ik}' A_{kj}' - \partial_i \partial_j p' + \nu \nabla^2 A_{ij}', \tag{6}$$

which is equivalent to the (3) for the total velocity gradient, thus allowing the direct use of models developed for the total velocity gradient in isotropic turbulence as an approximations for the unresolved velocity gradients.

Stochastic Model

The recent deformation of Gaussian fields (RDGF) stochastic model of Johnson & Meneveau (2016) is used to simulate the unresolved velocity gradients,

$$dA_{ij}' = \left(-A_{ik}' A_{kj}' - P_{ij} + V_{ij} \right) dt + dF_{ij}, \tag{7}$$

where $P_{ij} = \langle \partial_i \partial_j p' | \mathbf{A}' \rangle$ and $V_{ij} = \nu \langle \nabla^2 A_{ij}' | \mathbf{A}' \rangle$ represent the RDGF closure approximations in statistically stationary isotropic turbulence. These conditional averages are computed by treating the pressure p' and $\mathbf{A}'$ as slowly varying (approximately constant for a short time $\tau \sim \tau_\eta'$) along the Lagrangian trajectory, which determines the closure in terms of an upstream ('initial condition') closure and a short-time fluid deformation tensor given by the matrix exponential $D_{ij}^{-1} = [\exp(-\mathbf{A}'\tau)]_{ij}$. The RDGF closures for the conditional means are,

$$\begin{aligned} P_{ij} &= -\frac{C_{ij}^{-1}}{C_{kk}^{-1}} \mathrm{tr}\left(\mathbf{A}'^2\right) - \left(G_{ij} - \frac{C_{ij}^{-1}}{C_{kk}^{-1}} \mathrm{tr}(\mathbf{G}) \right), \\ V_{ij} &= \delta (T_{ij}' C_{kk}^{-1} + 2 T_{ik}' B_{kj}^{-1} - \frac{4}{21} B_{ik}^{-1} S_{kj}' - \frac{2}{21} B_{k\ell}^{-1} S_{k\ell}' \delta_{ij}), \end{aligned} \tag{8}$$

where the Gaussian fields calculation for the pressure Hessians enters through $G_{ij} = D_{mi}^{-1} \widehat{G}_{ij} D_{nj}^{-1}$, where,

$$\begin{aligned} \widehat{G}_{ij} = &\alpha \left(S_{mk}' S_{kn}' - \tfrac{1}{3} S_{k\ell}' S_{\ell k}' \delta_{mn} \right) \\ &+ \beta \left(\Omega_{mk}' \Omega_{kn}' - \tfrac{1}{3} \Omega_{k\ell}' \Omega_{\ell k}' \delta_{mn} \right) \\ &+ \gamma \left(S_{mk}' \Omega_{kn}' - \Omega_{mk}' S_{kn}' \right). \end{aligned} \tag{9}$$

The coefficients for $\widehat{\mathbf{G}}$ come from the Gaussian fields model: $\alpha = -2/7$, $\beta = -2/5$, $\gamma = 86/1365$, $\delta = -(7C_{kk})/(30\sqrt{15}\tau_\eta') \approx -0.06 C_{kk}/\tau_\eta'$. In the above expressions, the strain-rate $S_{ij}' = \left(A_{ij}' + A_{ji}' \right)/2$ and rotation-rate $\Omega_{ij}' = \left(A_{ij}' - A_{ji}' \right)/2$ are used along with the mixed tensor $T_{ij}' = \left(23 A_{ij}' + 2 A_{ji}' \right)/105$. The recent deformation enters through the left and right inverse Cauchy-Green tensors, $C_{ij}^{-1} = D_{ki}^{-1} D_{kj}^{-1}$ and $B_{ij}^{-1} = D_{ik}^{-1} D_{jk}^{-1}$.

The stochastic noise, $dF_{ij} = b_{ijk\ell} dW_{k\ell}$, uses a tensorial Wiener process characterized by zero mean and white-in-time correlation, i.e. $\langle dW_{ij} \rangle = 0$ and $\langle dW_{ij} dW_{k\ell} \rangle = \delta_{ik} \delta_{j\ell} dt$. The forcing is constrained to be isotropic and trace-free, with the resulting form,

$$\begin{aligned} b_{ijk\ell} = &-\frac{1}{3} \sqrt{\frac{D_s}{5}} \delta_{ij} \delta_{k\ell} + \frac{1}{2} \left(\sqrt{\frac{D_s}{5}} + \sqrt{\frac{D_a}{3}} \right) \delta_{ik} \delta_{j\ell} \\ &+ \frac{1}{2} \left(\sqrt{\frac{D_s}{5}} - \sqrt{\frac{D_a}{3}} \right) \delta_{i\ell} \delta_{jk}. \end{aligned} \tag{10}$$

The forcing coefficients D_s and D_a represent the diffusive growth rates for the symmetric and anti-symmetric part of the velocity gradient tensor caused by the forcing term, respectively. The three model parameters $\tau = 0.1302\tau_\eta'$, $D_s = 0.1014/\tau_\eta'^3$, and $D_a = 0.0505/\tau_\eta'^3$ are fixed by considering three exact constraints for homogeneous turbulence, namely, $2\langle S_{ij}' S_{ij}' \rangle = \tau_\eta'^{-2}$, $\langle Q' \rangle = 0$, $\langle R' \rangle = 0$. Note that the Gaussian closure depends in various ways on the Kolmogorov timescale, τ_η' which is a 'user input', i.e., the model can be run at any arbitrary τ_η'. More details on the development of the RDGF model described above have been given by Johnson & Meneveau (2016).

Determining the Dissipation Rate

Because τ_η' is a required input to the model, it must be determined from the coarse-grained field in the context of

LES. To that end, we employ a simple phenomenological model for the local dissipation rate along Lagrangian paths,

$$\frac{d\varepsilon}{dt} = \frac{\Pi - \varepsilon}{\tau_\varepsilon}, \tag{11}$$

where $\Pi = -\sigma_{ij}\widetilde{S}_{ij}$ is the production rate for sub-grid kinetic energy. This model is motivated by observations of the Lagrangian nature of the turbulent cascade (Meneveau & Lund, 1994; Wan *et al.*, 2010). The Lagrangian cascade timescale is established dimensionally: $\tau_\varepsilon^{-1} = C_\varepsilon \varepsilon^{1/3}(C_s\Delta)^{-2/3}$, where $C_\varepsilon = 0.5$ gives satisfactory results. In this paper, the SGS production, $\Pi = -\sigma_{ij}\widetilde{S}_{ij}$, is estimated using a Smagorinsky model (Smagorinsky, 1963) $\sigma_{ij} = -2(C_s\Delta)^2|\widetilde{S}|S_{ij}$, where $|\widetilde{S}| = \sqrt{2\widetilde{S}_{ij}\widetilde{S}_{ij}}$, so

$$\Pi = (C_s\Delta)^2|\widetilde{S}|^3. \tag{12}$$

In (11), ε is not necessarily a local value of dissipation but could be interpreted as the filtered dissipation rate $\varepsilon(\mathbf{x}) = 2\nu \iiint G(r;\Delta)|S'|^2(\mathbf{x}+\mathbf{r})d^3r$, which for a top-hat filter corresponds to the locally-averaged dissipation rate used in K62 phenomenology (Kolmogorov, 1962; Oboukhov, 1962). More strictly speaking, it functions as a time-dependent ensemble averaged dissipation given $\widetilde{S}(t)$ along a trajectory. Along a trajectory, the simple update formula

$$\varepsilon_{n+1} = \alpha\varepsilon_n + (1-\alpha)\Pi_{n+1}, \tag{13}$$

is used to solve (11), where $\alpha = \left[1 + C_\varepsilon\left(\varepsilon_n/(C_s\Delta)^2\right)^{1/3}\Delta t\right]^{-1}$. The input to the stochastic model for velocity gradients then uses $\tau'_\eta = \sqrt{\nu/\varepsilon}$, which changes in time along the trajectories.

Unsteady Consistency Constraint

Within this framework, the Kolmogorov timescale that the stochastic model sees will, in general, vary with time along each trajectory. Therefore, the model requires a slight adjustment to extend the consistency constraint, i.e. $\langle S'_{ij}S'_{ij}\rangle\tau'^2_\eta = 1/2$, to the case of unsteady Kolmogorov timescale, i.e. $d\tau'_\eta/dt \neq 0$. This can be done in a straightforward way which is applicable to any stochastic model which satisfies the consistency constraint for steady τ'_η.

Satisfaction of the consistency constraint for steady τ'_η implies that the dimensionless form of the model,

$$dA^*_{ij} = \left(-A^*_{ik}A^*_{kj} - P^*_{ij} + V^*_{ij}\right)dt^* + b^*_{ijk\ell}dW^*_{k\ell}, \tag{14}$$

satisfies the constraint $2\langle S^*_{ij}S^*_{ij}\rangle = 1$, where $A^*_{ij} = A_{ij}\tau_\eta$, $P^*_{ij} = P^*_{ij}\tau^2_\eta$, $V^*_{ij} = V_{ij}\tau^2_\eta$, $dt^* = dt/\tau_\eta$, $b^*_{ijk\ell} = b_{ijk\ell}\tau^{3/2}_\eta$, and $dW^*_{ij} = dW_{ij}/\tau^{1/2}_\eta$. An expedient method for extending the consistency constraint to unsteady Kolmogorov timescale is to simply allow τ_η be time-dependent in (14), thus generating an extra term by the product rule $dA^*_{ij} = \tau_\eta dA_{ij} + A_{ij}d\tau_\eta$. The resulting dimensional equation is then

$$dA'_{ij} = \left(-A'_{ik}A'_{kj} - P_{ij} + V_{ij} - \frac{1}{\tau'_\eta}\frac{d\tau'_\eta}{dt}A'_{ij}\right)dt + dF_{ij}. \tag{15}$$

The added linear term provides damping when τ'_η increase (dissipation locally decreasing) and amplification when τ'_η is decreasing (dissipation locally increasing) such that the model remains consistent with the definition of the local Kolmogorov timescale. This terms maintains consistency with derivation from the Navier-Stokes equations if we consider the closure approximation to be

$$-\langle\partial_i\partial_j p'|\mathbf{A}'\rangle + \nu\langle\nabla^2 A'_{ij}|\mathbf{A}'\rangle = -P_{ij} + V_{ij} - \frac{1}{\tau'_\eta}\frac{d\tau'_\eta}{dt}A'_{ij}, \tag{16}$$

which is consistent with the stationary isotropic turbulence models for $d\tau'_\eta/dt = 0$. Thus, the new term does not represent new physics, but only a practical extension of the model's constraints to the case of unsteady τ'_η.

NUMERICAL DETAILS

Channel Flow DNS and Filtering

The JHTDB channel flow dataset comes from a Navier-Stokes simulation in wall-normal velocity-vorticity form (Kim *et al.*, 1987) using a pseudo-spectral method in the horizontal plane and a seventh-order B-splines collocation method in the wall-normal direction (Lee *et al.*, 2013; Graham *et al.*, 2016). Every 5th timestep was written to disk for a total of 4000 snapshots, about one domain flow-through time. The simulation domain size was $8\pi \times 2 \times 3\pi$ with a resolution of $2048 \times 512 \times 1536$ in the streamwise (x), wall-normal (y), and spanwise (z) directions respectively. A third-order low-storage Runge-Kutta method was used for time advancement with $2/3$ truncation for de-aliasing (Orszag, 1971). Table 1 includes some details about the channel flow simulation, and more details can be found in the references herein.

Table 1. Details for the $2048 \times 512 \times 1536$ channel flow dataset at $Re_\tau = 1000$ used here (Graham *et al.*, 2016).

h	ν	u_*	U_{bulk}	δx^+	δz^+	δt
1	5e-5	5e-2	1.00	12.3	6.1	1.3e-3

To mimic a large-eddy simulation, the DNS channel flow database was filtered using a trapezoidal rule box filter of size 32 times the grid spacing, i.e. $\Delta_x = 32\delta x$ and similar for y and z. The filter width for the model is specified as $\Delta = \left(\Delta_x\Delta_y\Delta_z\right)^{1/3}$. The filtered data was stored on a grid 16 times as coarse in each direction, including 16 times as coarse in time. The size of the coarse-grained dataset was thus $128 \times 32 \times 96$ with 250 timesteps. This reduced the volume of the dataset by a factor of 2^{16}, from ~ 100 TB to ~ 1 GB, which was stored on a local desktop computer for analysis. The first grid point off the wall was at $y^+ \approx 8$ in the filtered dataset, which would be difficult in practice for a large-eddy simulation to imitate. Because the original DNS grid was non-uniform in the wall-normal direction, the technique used here resulted in a non-uniform grid for the filtered dataset as well as a slight spatial dependence of the filter kernel, which is ignored for convenience in the governing equations. Figure 1 shows the unfiltered and filtered velocity fields from the centerplane of the channel.

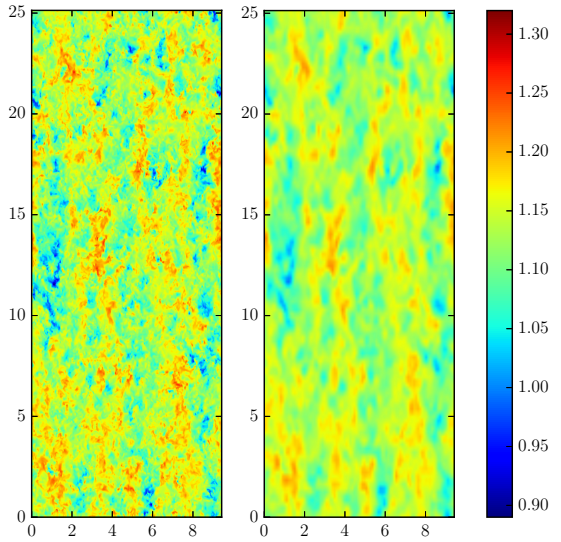

Figure 1. Colormaps of instantaneous streamwise velocity on the centerplane of the channel flow from full DNS (left) and coarse-grained DNS (right).

Stochastic Model

The stochastic model was computed using a second-order accurate predictor-corrector method. The time step taken was $\delta t = 0.0065$, which is 5 times the DNS simulation timestep and about $1/100$th of the centerline Kolmogorov timescale. Coarse-grained velocity gradients from the filtered database, used for determining τ'_η, were computed using second-order central differencing with tri-linear spatial interpolation and linear temporal interpolation.

The Smagorinsky coefficient C_s was given a fixed value depending on wall normal distance (Porté-Agel *et al.*, 2000), $C_s = C_{s,0}/\sqrt{1+\left((C_{s,0}\Delta)/(\kappa y)\right)^2}$, where $\kappa = 0.41$ is used for the Karman constant. The model with the choice $C_{s,0} = 0.19$ was found to accurately reproduce profiles of $\langle \Pi | y \rangle$ when compared with the SGS production computed from filtering the DNS database. For this low-Re case, we use a non-equilibrium correction replacing Π from (12) with $C_{neq}(y)\Pi$ before substituting into (13). The low-Re correction factor is determined from the DNS results as $C_{neq}(y) = \langle \varepsilon | y \rangle / \langle \Pi | y \rangle$ so that energy is injected into small scale dynamics with the correct wall-normal profile. In practice, for higher Re simulations, such a correction is expected to be small, $C_{neq} \approx 1$. Alternatively, a more sophisticated model than (11) for ε could be developed for more complex flows in future studies.

Particle Initial Conditions

To demonstrate the proposed stochastic model for the unresolved velocity gradients, we wish to avoid the near-wall region as much as possible, because additional modeling (a topic not pursued in this paper) will be necessary there. For this reason, 43200 Lagrangian tracer particles are released at random (x,z) position at the channel center at $t = 0$. Over the course of time, they disperse from the low dissipation region in the center into regions of increasing velocity gradient strengths closer to the walls. Ensemble statistics, including those conditioned on wall-normal position and time, are used to judge the accuracy of the proposed model. Prior to releasing the particles, the velocity gradient stochastic model is initialized with Gaussian statistics having the correct τ'_η and given a start-up run time of 1000 timesteps before $t = 0$ for which they have a constant τ'_η equal to the value at $t = 0$. The initial value of τ'_η is determined assuming a balance of production and dissipation, but correcting for the low-Re non-equilibrium effect: $\varepsilon(t=0) = C_{neq}(y=0)\Pi(t=0)$.

RESULTS

We first check to see if the proposed model can correctly account for the variation of velocity gradient magnitudes in space and time as the particles disperse from the centerline of the channel. Figure 2 shows as a function of time the dissipation timescale, $\tau_\eta = \sqrt{\nu/\langle\varepsilon\rangle}$, where brackets denote ensemble averaging over all trajectories regardless of wall-normal location. It is evident that the stochastic model provides good agreement in terms of the magnitude of velocity gradients produced, which validates the use of Π from the Smagorinsky model with (11) to determine the local dissipation rate, with the help of tuning $C_{s,0} = 0.19$ as well as the low-Re non-equilibrium correction using DNS. The local maximum in timescale (minimum in dissipation rate) near $t = 5$ which appears in the DNS data (dashed line) is captured by the model, where setting the factor $C_\varepsilon = 0.5$ for (11) is important for correctly capturing this effect. The timescale drops as time continues, however, because the particles move closer to the wall and experience regions of more intense turbulence (higher dissipation rate).

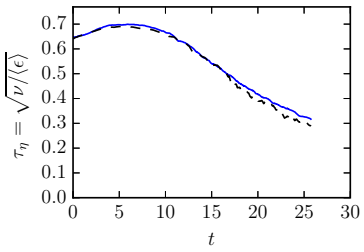

Figure 2. Comparison of DNS Kolmogorov timescale for total dissipation (blue line) with Kolmogorov timescale using (11) for unresolved dissipation (green), RDGF stochastic model timescale (black dashed), and total filtered DNS + RDGF timescale (black solid).

To explore the spatial dependence of velocity gradient magnitudes, Figure 3 shows Kolmogorov timescales, $\tau_\eta(y) = \sqrt{\nu/\langle\varepsilon|y\rangle}$, constructed using the dissipation averaged over the trajectory ensemble conditionally on wall-normal position. Two different times are shown: $t = 11.7$ and $t = 23.4$. At the first time, a few particles have started to reach the wall while most remain in the bulk of the channel. The second time is close to the end of the DNS data, where particles are closer to a uniform distribution. Near the centerline, the lower turbulence intensities lead to lower velocity gradient magnitudes while the velocity gradients are more intense approaching either walls.

Now that the magnitude of the velocity gradient tensor fluctuations has been shown to be accurately reproduced, we exploit a unique benefit of the stochastic model to explore the tensorial structure of the full velocity gradient. In the following discussion, statistics taken over the trajectories for the entire time of the simulation are considered so

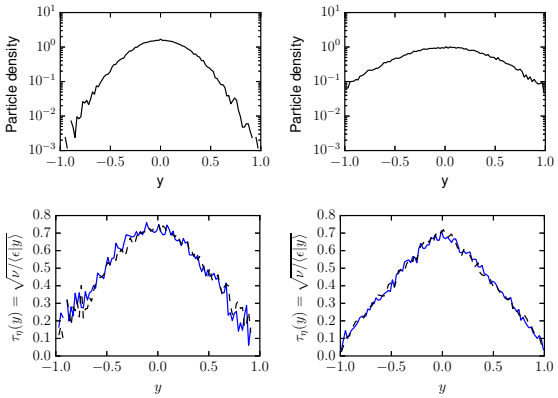

Figure 3. Particle density (top) and Kolmogorov timescale (bottom) as a function of y using conditionally averaged dissipation $\langle\varepsilon|y\rangle$, at time $t = 11.7$ (left) and time $t = 23.4$ (right). For $\tau_\eta(y)$, dashed (black) lines represent DNS results and solid (blue) lines those of the stochastic model.

to aid statistical convergence.

Figure 4 compares the results of the stochastic model with DNS statistics for the PDF in Q-R space. The statistics for these plots are taken over the whole ensemble for all timesteps as the particles spread out from the centerline of the channel. The characteristic teardrop shape from isotropic turbulence is evident in both results, and the stochastic model provides an excellent match to the DNS results. This shows that the unique statistical signature of velocity gradient tensor invariants is captured by the model.

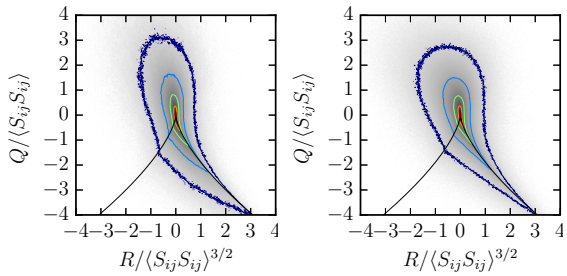

Figure 4. Logarithmically spaced iso-contours (10^1, 10^0, 10^{-1}, 10^{-2}, 10^{-3}) of the joint-PDF in Q-R space for trajectory ensemble in channel flow using DNS (left) and filtered DNS with RDGF (right).

The probability distributions of dissipation and enstrophy are shown in Figure 5. For both of these two quantities, the model results display the well-known stretched-exponential form with slightly over-predicted probabilities in the tails. Nonetheless, the agreement is quite good between the model and DNS. Figure 6 shows alignment statistics for the velocity gradient tensor. The left plot compares the alignments for the vorticity vector with the three strain-rate eigenvectors, arranged in decreasing order according to their associated eigenvalue. The DNS trends are well-represented by the stochastic model, including the alignment with the intermediate eigenvalue, anti-alignment with the compressive eigenvalue, and approximately uniform PDF with the stretching direction. The PDF of $s^* = -3\sqrt{6}\Lambda_1\Lambda_2\Lambda_3/\left(\Lambda_1^2+\Lambda_2^2+\Lambda_3^2\right)^{3/2}$ is shown on the right. Again, excellent agreement is seen between DNS and the stochastic model. Figure 7 shows the PDF for individual components of the velocity gradient tensor. Stretched-exponential tails are seen for both DNS and the stochastic model. As with the dissipation and enstrophy PDFs, the stochastic model only slightly over-predicts the probabilities of rare events and the overall agreement is quite good.

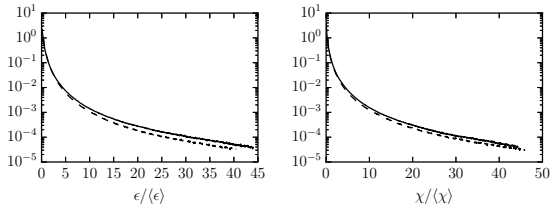

Figure 5. PDFs of dissipation (left) and enstrophy (right) normalized by their mean values. Solid lines show stochastic model results, dashed lines show DNS results.

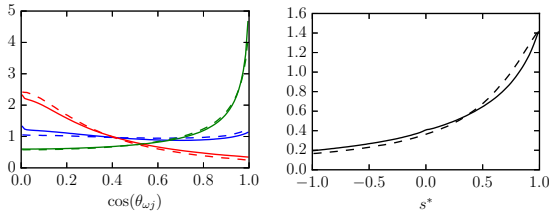

Figure 6. PDFs of alignment between vorticity and strain-rate eigenvalues (left) as well as of s^* (right). Solid lines indicate stochastic model results and dashed lines show DNS results.

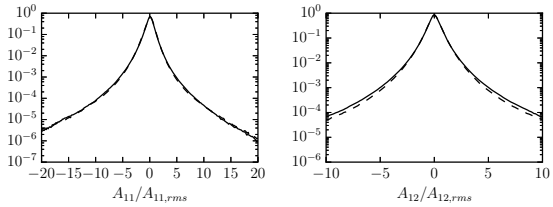

Figure 7. PDFs of longitudinal (left) and transverse(right) velocity gradient components. Solid lines indicate stochastic model results and dashed lines show DNS results.

DISCUSSION

The paper introduces the use of stochastic models for Lagrangian velocity gradients in isotropic turbulence as a means for accessing small-scale statistics in a coarse-grained simulation. The approach is demonstrated using a filtered DNS database of a turbulent channel flow with Lagrangian tracers released from the centerline of the channel and dispersing toward the walls. The Recent Deformation of Gaussian Fields (RDGF) closure is used to simulate the dynamics of the velocity gradient tensor. To use this approach with LES, it is necessary to provide a local dissipation timescale from the information available in the coarse-grained field. For an *a priori* evaluation of the RDGF closure in a channel flow, the simple time-filtered model, (11), suffices provided some information from the

DNS. This is the key ingredient for matching velocity gradient magnitudes, i.e. obtaining a reliable estimate of local dissipation rate from the coarse-grained field. The approach here, validated in Figures 2 and 3 relies on tuning $C_\varepsilon = 0.5$ (which may or may not work well for other flows) as well as a DNS-informed local non-equilibrium correction for $\langle \Pi | y \rangle \neq \langle \varepsilon | y \rangle$. It is likely that the non-equilibrium correction is less necessary at higher Reynolds numbers. Nonetheless, an alternative approach using a transport equation for ε could be constructed similar to k-ε models for RANS simulations, perhaps providing more fidelity than (11) without a non-equilibrium correction. Once this is accomplished, the results in Figures 4-7 illustrate the both the fidelity of the stochastic model for the velocity gradient and the similarity between velocity gradient statistics in the channel flow with isotropic turbulence.

REFERENCES

Cantwell, B. J. 1992 Exact solution of a restricted Euler equation for the velocity gradient tensor. *Phys. Fluids* **4** (4), 782–793.

Chen, J., Jin, G. & Zhang, J. 2016 Large eddy simulation of orientation and rotation of ellipsoidal particles in isotropic turbulent flows. *J. Turbul.* **5248** (June), 1–19.

Chertkov, M., Pumir, A. & Shraiman, B. I. 1999 Lagrangian tetrad dynamics and the phenomenology of turbulence. *Phys. Fluids* **11** (8), 2394–2410.

Chevillard, L. & Meneveau, C. 2006 Lagrangian Dynamics and Statistical Geometric Structure of Turbulence. *Phys. Rev. Lett.* **97** (17), 174501.

De Tullio, M. D., Nam, J., Pascazio, G., Balaras, E. & Verzicco, R. 2012 Computational prediction of mechanical hemolysis in aortic valved prostheses. *Euro J Mech. B* **35**, 47–53.

Graham, J., Kanov, K., Yang, X. I. A., Lee, M. K., Malaya, N., Burns, R., Eyink, G., Moser, R. D. & Meneveau, C. 2016 A Web Services-accessible database of turbulent channel flow and its use for testing a new integral wall model for LES DNS Approach and Simulation Parameters. *J. Turbul.* **17** (2), 181–215.

Jeong, E. & Girimaji, S. S. 2003 Velocity-Gradient Dynamics in Turbulence: Effect of Viscosity and Forcing. *Theoret. Comput. Fluid Dyn.* **16** (6), 421–432.

Johnson, P. L. & Meneveau, C. 2016 A closure for Lagrangian velocity gradient evolution in turbulence using recent deformation mapping of initially Gaussian fields. *J. Fluid Mech.* **804**, 387–419.

Karp-Boss, L, Boss, E & Jumars, P A 1996 Nutrient Fluxes to Planktonic Osmotrophs in the Presence of Fluid Motion. *Oceanography and Marine Biology: An Annual Review* **34**, 71–107.

Kim, J., Moin, P. & Moser, R. 1987 Turbulence statistics in fully developed channel flow at low Reynolds number. *J. Fluid Mech.* **177**, 133–166.

Kolmogorov, A. N. 1941 The local structure of turbulence in incompressible viscous fluid for very large Reynolds numbers. *Dokl. Akad. Nauk SSSR* **30**, 299–303.

Kolmogorov, A. N. 1962 A refinement of previous hypotheses concerning the local structure of turbulence in a viscous incompressible fluid at high Reynolds number. *J. Fluid Mech.* **13** (01), 82–85.

Lee, M., Malaya, N. & Moser, R. D. 2013 Petascale direct numerical simulation of turbulent channel flow on up to 786K cores. In *Intl Conf for High Perf Comput*. New York, NY: ACM Press.

Maffettone, P.L. & Minale, M. 1998 Equation of change for ellipsoidal drops in viscous flow. *J. Non-Newtonian Fluid Mech.* **78** (2-3), 227–241.

Marchioli, C. & Soldati, A. 2015 Turbulent breakage of ductile aggregates. *Phys. Rev. E* **91** (5), 1–8.

Martin, J., Dopazo, C. & Valino, L. 1998 Dynamics of velocity gradient invariants in turbulence: Restricted Euler and linear diffusion models. *Phys. Fluids* **10** (8), 2012.

Maxey, M. R. 1987 The gravitational settling of aerosol particles in homogeneous turbulence and random flow fields. *J. Fluid Mech.* **174**, 441.

Mazzitelli, I. M., Toschi, F. & Lanotte, A. S. 2014 An accurate and efficient Lagrangian sub-grid model. *Phys. Fluids* **26** (9), 095101.

Meneveau, C. 2011 Lagrangian Dynamics and Models of the Velocity Gradient Tensor in Turbulent Flows. *Ann. Rev. Fluid Mech.* **43**, 219–245.

Meneveau, C. & Lund, T. S. 1994 On the lagrangian nature of the turbulence energy cascade. *Phys. Fluids* **6** (8), 2820–2825.

Oboukhov, A. M. 1962 Some specific features of atmospheric tubulence. *J. Fluid Mech.* **13** (01), 77–81.

Orszag, S. A. 1971 On the elimination of aliasing in finite difference schemes by filtering high-wavenumber components. *J. Atmosph. Sci.* **28**, 1074.

Park, G. I., Urzay, J., Bassenne, M. & Moin, P. 2015 A dynamic subgrid-scale model based on differential filters for LES of particle-laden turbulent flows. *CTR Ann Res Briefs* pp. 17–26.

Pope, S. B. 2000 *Turbulent Flows*. Cambridge, UK: Cambridge University Press.

Porté-Agel, F., Meneveau, C. & Parlange, M. B. 2000 A scale-dependent dynamic model for large-eddy simulation: application to a neutral atmospheric boundary layer. *J. Fluid Mech.* **415** (2000), 261–284.

Pumir, A. & Wilkinson, M. 2011 Orientation statistics of small particles in turbulence. *New J. Physics* **13**.

Sagaut, P. 2006 *Large Eddy Simulation for Incompressible Flows*, 3rd edn. Springer-Verlag.

Sawford, B. 2001 Turbulent relative dispersion. *Ann. Rev. Fluid Mech.* **33**, 289–317.

Smagorinsky, J. 1963 General Circulation Experiments With the Primitive Equations. *Monthly Weather Review* **91** (3), 99–164.

Sreenivasan, K. R. & Antonia, R. A. 1997 The Phenomenology of Small-Scale Turbulence. *Ann. Rev. Fluid Mech.* **29** (1), 435–472.

Vieillefosse, P. 1982 Local interaction between vorticity and shear in a perfect incompressible fluid. *J. Physique* **43**, 837–842.

Vieillefosse, P. 1984 Internal motion of a small element of fluid in an inviscid flow. *Physica A* **125**, 150–162.

Voth, G. A. & Soldati, A. 2017 Anisotropic Particles in Turbulence. *Ann. Rev. Fluid Mech.* .

Wan, M., Xiao, Z., Meneveau, C., Eyink, G. L. & Chen, S. 2010 Dissipation-energy flux correlations as evidence for the Lagrangian energy cascade in turbulence. *Phys. Fluids* **22** (6), 061702.

White, C. M. & Mungal, M. G. 2008 Mechanics and Prediction of Turbulent Drag Reduction with Polymer Additives. *Ann. Rev. Fluid Mech.* **40** (1), 235–256.

Wilczek, M. & Meneveau, C. 2014 Pressure Hessian and viscous contributions to velocity gradient statistics based on Gaussian random fields. *J. Fluid Mech.* **756**, 191–225.